Utility of BRDF Models for Estimating Optimal View Angles in Classification of Remotely Sensed Images *

P. F. Valdez[a] and G. W. Donohoe[a]

[a]NASA ACE Center for Autonomous Control Engineering
Electrical and Computer Engineering
University of New Mexico
Albuquerque, New Mexico 87131-1356 USA
pvaldez@eece.unm.edu   donohoe@eece.unm.edu

1. Introduction

Statistical classification of remotely sensed images attempts to discriminate between surface cover types on the basis of the spectral response recorded by a sensor. It is well known[1-3] that surfaces reflect incident radiation as a function of wavelength producing a spectral signature specific to the material under investigation. Multispectral and hyperspectral sensors sample the spectral response over tens and even hundreds of wavelength bands to capture the variation of spectral response with wavelength. Classification algorithms then exploit these differences in spectral response to distinguish between materials of interest. Sensors of this type, however, collect detailed spectral information from one direction (usually nadir); consequently, do not consider the directional nature of reflectance potentially detectable at different sensor view angles.

Improvements in sensor technology have resulted in remote sensing platforms capable of detecting reflected energy across wavelengths (spectral signatures) and from multiple view angles (angular signatures) in the fore and aft directions. Sensors of this type include: the moderate resolution imaging spectroradiometer[4] (MOD IS), the multiangle imaging spectroradiometer[5] (MIS R), and the airborne solid-state array spectroradiometer[6] (AS AS).

A goal of this paper, then, is to explore the utility of BRDF models in the selection of optimal view angles for the classification of remotely sensed images by employing a strategy of searching for the maximum difference between surface BRDFs. After a brief discussion of directional reflectante in Section 2, attention is directed to the Beard-Maxwell BRDF model and its use in predicting the bidirectional reflectance of a surface. The selection of optimal viewing angles is addressed in Section 3, followed by conclusions and future work in Section 4.

1.1. NEFDS Spectral Database

A collection of spectral datasets was obtained from the National Imagery Resource Library (NIRL) and used in this study. Intimately related to the Materials Exploitation Database (MED), the Spectrum Archival Library (SAL), and the Spectral Catalog,[7] the Nonconventional Exploitation Factors Data System (NEFDS) database is composed of spectral reflectante measurement data in the visible/near-infrared (VNIR), the mid-infrared (MIR) and combined visible/near-mid-infrared (VNMIR) for samples of selected materials.

Spectral samples of a concrete runway, a galvanized steel rooftop, and a couple of painted surfaces in the visible/near-infrared (VNIR) were selected for input to a BRDF model for the pairwise estimation of optimal view angles in the classification of remotely sensed images. Detailed properties of the materials used in this analysis have been assembled and are presented in the Spectral Catalog cited earlier.

2, **Directional Reflectance**

The *directional–hemispherical* reflect ante defined as

$$\rho'_{dh} = \frac{d\Phi_r}{d\Phi_i} \tag{1}$$

is the fraction of incident radiant flux density from direction, (θ_i, ϕ_i) that is reflected by the surface into all possible directions of the hemisphere surrounding the sample. By definition, then, ρ'_{dh} does not provide any information on the directional nature of reflectance and is only adequate for surfaces that reflect isotropically.

Many surface materials of interest, however, are anisotropic reflectors so that the spectral response is also dependent on the viewing geometry of the sensor.[8-10] This fact has lead to classification difficulties in which single view imagery was used to discriminate between surface materials.[11] A more general and useful description for the directional nature of reflected radiant flux is contained in the *bidirectional reflectance distribution function* (BRDF) which relates the directional distribution of exitant flux to the incident radiant flux striking the surface.
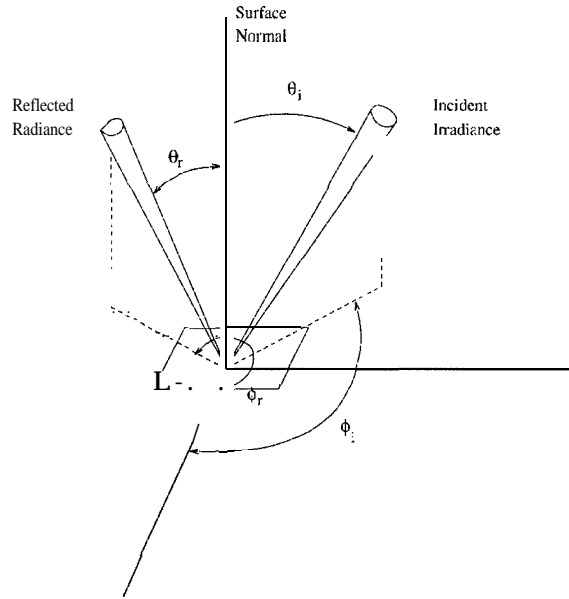
2.1. **Bidirectional Reflectance**

Figure 1. Co-ordinate System Defining Solar Angles and Sensor Viewing Angles.

The BRDF is a function of four angles (Figure 1) and is defined as the ratio of reflected radiance from a surface to the irradiance incident to the surface from an illuminating source. This relationship is seen in Equation 2

$$\rho'_{bd}(\Theta_i, \Theta_r; \lambda) = \frac{dL_r(\Theta_i, \Theta_r; \lambda)}{dE_i(\Theta_i; \lambda)} \tag{2}$$

where the dependence on incident angles, $\Theta_i = \{\theta_i, \phi_i\}$, exit ant angles, $\Theta_r = \{9,, \phi_r\}$, and wavelength, λ, is shown.

754

2.2. BRDF Models

Reflection of light from a surface is a complex phenomenon which can be very difficult to explain and accurately predict. Even with a firm grasp of the physics involved, the dynamics of a changing environment complicates matters so that a complete understanding is often not possible. As a result, several types of BRDF models have emerged; those based on first principles such as radiative transfer theory,[12–14] geometrical optics ,[15,16] physical optics (wave theory of light) and those that fit analytic equations to the observed reflectance.[17]

Two mechanisms of reflect ante are generally identified: surface and subsurface (volumetric) reflect ante. Surface reflect ante occurs at the interface between materials; usually the air-material interface and can be quite anisotropic. Subsurface reflectance is typically isotropic and occurs when incident light penetrates the surface and collides with inhomogeneities (such as paint pigments) suspended in the substrate. For rough matte surfaces, the observed reflectance is usually diffuse (Lambertian) and therefore nondirectional. The BRDF in this case is independent of both the incident and exitant directions and can be expressed as

$$\rho'_{bd}(\Theta_i, \Theta_r; \lambda) \equiv \rho'_{bd}(\lambda). \tag{3}$$

Perfectly smooth planar surfaces on the other hand behave as specular reflectors that reflect light in the critical mirror angle only. In this instance, the BRDF is highly dependent on the incoming and outgoing directions and can be expressed as a Dirac distribution.[18] Most practical surface mat erials are somewhere between the two extremes of diffuse and specular reflectors. Therefore, BRDF models typically represent the surface reflectance in terms of both a diffuse component and a specular component.

The aim of BRDF models, then, is to predict the reflectance behavior of surfaces under conditions of incident radiant energy striking the surface from various directions. One such model is the Beard-Maxwell BRDF model.

2,2.1. Beard- Maxwell BRDF

The Beard-Maxwell (B-M) BRDF model[19] was originally developed to characterize the reflectance properties of painted surfaces but has been used successfully in estimating the reflectance of other surfaces as well. Empirically based, this model has seven input parameters that are derived from a series of reflectance measurements collected under the controlled conditions of a laboratory setting.

A functional description of the B-M BRDF model is specified by Equation 4

$$\rho'_{bd}(\Theta_i, \Theta_r) = \frac{R(\beta)}{R(0)} \frac{\rho_{fs} \cos^2 \theta_N}{\cos\theta_i \cos\theta_r} \left[\frac{1 + \theta_N}{1 + \frac{\theta_N}{\Omega} e^{-2\beta/\tau}} \right] + \rho_d + \frac{2\rho_v}{\cos\theta_i + \cos\theta_r} \tag{4}$$

where the first term in Equation 4 is the first surface reflectance attenuated by the shadowing and obscuration function enclosed in square brackets. The second term, ρ_d, is the diffuse (Lambertian) component and the third term is the component due to subsurface volumetric scattering.

3. Selection of Optimal Viewing Angles

In this section, the utility of BRDF models in the selection of optimal viewing angles for classification of remotely sensed images is explored. To motivate this discussion, consider the B-M BRDF of a galvanized steel rootop surface generated under the following conditions: the material is oriented in a horizontally flat position (θ_{matl} = 00), the solar position is specified by a zenith
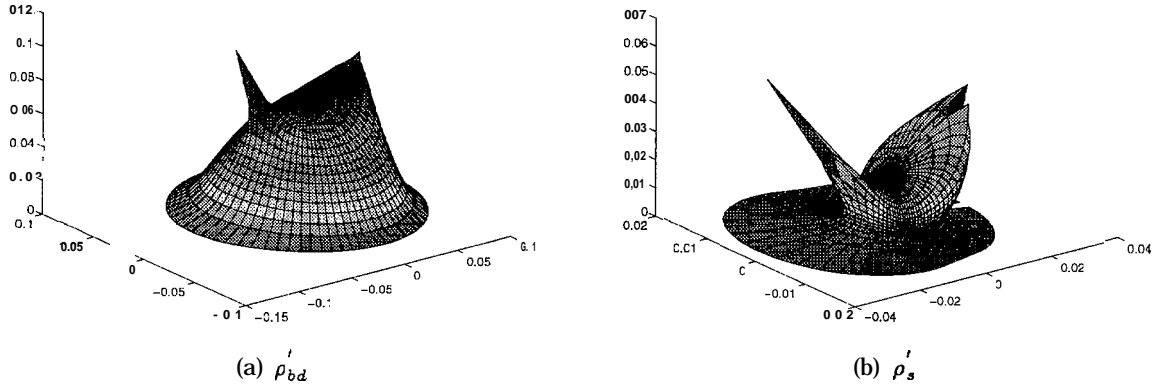
755

(a) ρ'_{bd} (b) ρ'_s

Figure 2. B-M BRDF:0526stla (galvanized steel rooftop)

angle of $\theta_i = 30°$ and an azimuth of $\phi_i = 0°$, with the BRDF evaluated at a spectral wavelength of $\lambda = 0.635\mu m$. Note that the observed BRDF seen in Figure 2(a) is dependent on viewing angles in both the azimuth and zenith directions due to forward scattering (sharp peak on the left) and backward scattering (peak on the right) effects. These effects are also seen in the surface component of the B-M BRDF shown in Figure 2(b) where once again the forward scattering peak is sharp and to the left with a significant backscattering lobe directed toward the solar position. Analagous to the variation in spectral signatures among material types, the spatial distribution of reflectance with angle gives rise to angular signatures specific to material type. Differences in angular signature can lead to an increased ability to distinguish between materials if identified and incorporated into a classification system. Our goal, then, is to identify regions of maximum difference between angular signatures through the use of the B-M BRDF model.

The B-M BRDF of several surfaces was generated with the the material positioned horizontally flat, the solar position given by a zenith of $\theta_i = 30°$ and an azimuth of $\phi_i = 0$"; wavelength ranged from 0.3- 1.0 μm in increments of 0.005 μm. Positioning of the sensor varied from $\phi_r = 0$" to $\phi_r = 180°$ in the azimuthal direction at 5° increments and in the zenith from $\theta_r = 0°$ to $\theta_r = 65°$ every 5° corresponding to each azimuthal direction. As an illustration, B-M BRDF surfaces of a galvanized steel rooftop with the sensor positioned at an azimuth of $\phi_r = 180°$ and $\phi_r = 175°$ are shown in Figures 3(a) and 3(b), respectively. Under similar conditions, B-M BRDF surfaces were generated for an aluminum painted low emissivit y green surface (0537 UUUPNT), a gray unweathered polyurethane paint on aircraft surface (0741 UUUPNT), and a concrete runway surface (0671 UUUCNC).

Pairwise separability was then computed on the basis of a pointwise root-squared (rs) difference between B-M BRDF surfaces of each material. Therefore, corresponding to each azimuth direction a root-squared difference surface was determined as shown in Figure 4(a). Inspection of the rs difference surface indicates that the maximum difference occurs in the zenith direction of $\theta_r = 30°$. A cross-section of the surface along $\theta_r = 30°$ (Figure 4(b)) further shows that the maximum rs difference is achieved in the shorter wavelengths around $0.4\mu m$ and decreases as wavelength gets longer. A similar analysis in each azimuthal direction, $\phi_r = \{0, 5, 10, ...60,65\}$, resulted in the maximum difference between BRDF surfaces occuring at $\phi_r = 0°$, $\theta_r = 30°$, and in the wavelength range of $0.4 - 0.5\mu m$.

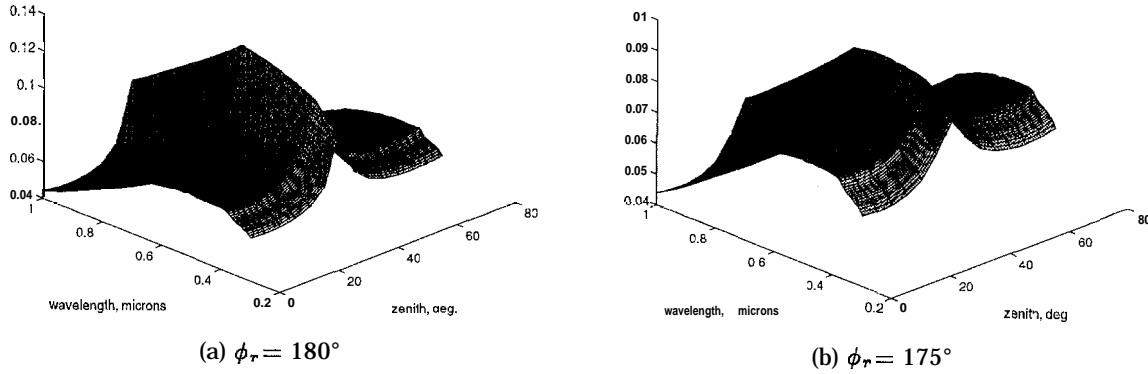A separability analysis to determine the optimal viewing conditions for discrimination between

756

(a) $\phi_r = 180°$ (b) $\phi_r = 175°$

Figure 3. B-MBRDF Surface: 0526UUUSTLa (galvanized steel rooftop)

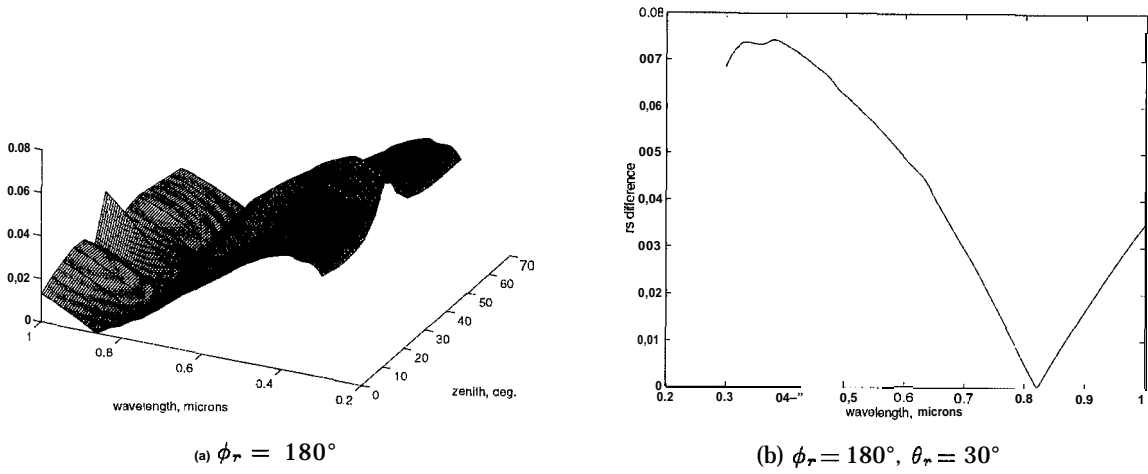(a) $\phi_r = 180°$ (b) $\phi_r = 180°$, $\theta_r = 30°$

Figure 4. Pointwise Difference Surface: 0526 UUUSTLa (galvanized steel rooftop) and 0537UU-UPNT (green painted aluminum surface)

a concrete runway (0671 UUUCNC) and a painted aircraft surface (0741 UUUPNT) was also conducted. Results indicated that the maximum rs difference occurred in the primary backscatter direction, $\phi_r = 0°$ and optimal θ_r in the range $20° - 40°$. Additional analysis indicated that the optimal wavelength range for discrimination, however, was in the longer wavelengths from approximately 0.8 μm to 1.0 pm.

4. Conclusions and Future Work

The utility of BRDF models for pairwise discrimination between surface materials through the selection of optimal view angles was explored. Employing a strategy of maximum rs difference between the respective BRDFs to indicate maximum separability, several cases were considered of which two were reported in this paper. In every case studied, the maximum rs difference occurred in the principal plane of the Sun with the BRDF due to backscatter effects yielding a slightly greater separability than the forward scattering direction.

It should be noted, however, that there were several limitations in this preliminary study: our analysis at this point was qualitative, atmospheric effects were completely ignored (we expect that these effects are not significant at low altitues but could be extremely important at high altitudes), and only one solar position was considered.

Future efforts will concentrate on quantifying the search for optimal viewing angles, incorporating atmospheric effects, and exploring the affect that solar position has on the separability y between surface BRDFs.

REFERENCES

1. P. H. Swain and S. M. Davis, *Remote Sensing: The Quantitative Approach*, McGraw-Hill, 1st.ed., 1978.
2. T. M. Lillesand and R. W. Kiefer, *Remote Sensing and Image Interpretation*, John Wiley & Sons, Inc., 3rd cd., 1994.
3. J. A. Richards, *Remote Sensing Digital Image Analysis: An Introduction,* Springer-Verlag, 1st. cd., 1986.
4. P. E. Ardanuy, D. Han, and V. V. Salomonson, "The moderate imaging spectrometer (modis) science and data system requirements," *IEEE Trans. on Geosci Remote Sensing* GE-29, pp. 75-88, Jan. 1991,
5. D. J. Diner and et al., "Misr: A multiangle imaging spectroradiometer for geophysical and climatological research from eos," *IEEE Trans. on Geosci Remote Sensing 27,* pp. 200-214, 1989.
6. J. R. Irons, K. J. Ranson, D. L. Williams, R. R. Irish, and F. G. Huegel, "An off-nadir-pointing imaging spectroradiometer for terrestrial ecosystem studies," *IEEE Trans. on Geosci Remote Sensing* GE-29, pp. 66–74, Jan. 1991.
7. National Photographic Interpretation Cent er, *Spectral Catalog Version 4.0*, Jan. 1993.
8. B. Holben and R. S. Fraser, "Red and near-infrared sensor response to off-nadir viewing," *Int. J. Remote Sens. 5,* pp. 145-160, 1984.
9. B. Holben and D. Kimes, "Directional reflectance response in avhrr red and near-ir bands for three cover types and varying atmospheric conditions," *Remote Sens. Environ. 32,* pp. 213-236, 1986.
10. R. D. Jackson, P. M. Teillet, P. N. Slater, G. Fedosejevs, M. F. Jasinski, J. K. Aase, and M, S. Moran, "Bidirectional measurements of surface reflectance for view angle corrections of oblique imagery," *Remote Sens. Environ. 32,* pp. 763–766, Nov. 1976.
11. G. M. Foody, "The effects of viewing geometry on image classification," *Int. J. Remote Sensing 9(12), pp. 1090–1915, 1988.*
12. D, S. Kimes and J. A. Kirchner, "Radiative transfer model for heterogeneous 3-d scenes," *Applied Optics 21, pp. 4119–4129,* Nov. 1982.
13. S. A. W. Gerstl and C. Simmer, "Radiation physics and modelling for off-nadir satellite-sensing of non-lambertian surfaces," *Remote Sens. Environ. 20,* pp. 1-29, 1986.
14. B. Pinty, M. M. Verstraete, and R. E. Dickinson, "A physical model for predicting bidirectional reflectances over bare soil," *Journal of Geophysical Research 27,* pp. 273–288, 1989.
15. K. E. Torrance and E. M. Sparrow, "Theory for off-specular reflection from roughened surfaces," *J. Opt. Sot, Am, 57,* pp. 1105-1114, Sept. 1967.
16. X. Li and S. A. H., "Geometrical-optical bidirectional reflectance modelling of a conifer forest canopy," *IEEE Trans. on Geosci* Remote Sensing GE-24, pp. 906-919, 1986.
17. C. L. Walthall, J. M. Norman, J. M. Welles, G. Campbell, and B. L. Blad, "Simple equation to approximate e the bidirectional reflectance from vegetative canopies and bare soil surfaces ," *Applied Optics* 24, pp. 383–387, Feb. 1985.
18. W. G. Rees, *Physical Principles of Remote Sensing,* Cambridge University Press, 1st. cd., 1990.
19. J. Beard and J. R. Maxwell, "Bidirectional reflect ante model validation and utilizat ion," Technical Report TR-73-303, AFAL, Oct. 1973.